Detecting striations via the lateral photovoltage scanning method without screening effect

S. Kayser[1] · P. Farrell[1] · N. Rotundo[2]

Abstract

The lateral photovoltage scanning method (LPS) detects doping inhomogeneities in semi-conductors such as Si, Ge and Si_xGe_{1-x} in a cheap, fast and nondestructive manner. LPS relies on the bulk photovoltaic effect and thus can detect any physical quantity affecting the band profiles of the sample. LPS finite volume simulation using commercial software suffer from long simulation times and convergence instabilities. We present here an open-source finite volume simulation for a 2D Si sample using the `ddfermi` simulator. For low injection conditions we show that the LPS voltage is proportional to the doping gradient. For higher injection conditions, we directly show how the LPS voltage and the doping gradient differ and link the physical effect of lower local resolution to the screening effect. Previously, the loss of local resolution was assumed to be only connected to the enlargement of the excess charge carrier distribution.

Keywords Lateral photovoltage scanning method (LPS) · Semiconductor simulation · Van Roosbroeck system · Finite volume simulation · Crystal growth

1 Introduction

Semiconductor crystals are the very basis for any (opto)electronic component such as transistors, LEDs or solar cells. To grow crystals, two well-established techniques dominate the market for single crystalline silicon. On the one hand, Czochralski grown crystals (95%

✉ P. Farrell
farrell@wias-berlin.de

S. Kayser
stefan.kayser@wias-berlin.de

1 Weierstraß-Institut für angewandte Analysis und Stochastik, Mohrenstr. 39, 10117 Berlin, Germany

2 University of Florence, Dipartimento di Matematica e Informatica Ulisse Dini, Viale Morgagni 67/A, 50134 Firenze, Italy

market share) are cheap to produce but systematically introduce oxygen and carbon into the crystal, thus limiting their quality severely Zulehner (1994). On the other hand, floating zone crystals (5% market share) produce purer crystals, however, significantly increase the production cost Becker et al. (2010).

In order to improve the crystal growth design, it is crucial to predict the temperature distribution of the coils which heat up the raw material. Along the solid-liquid interface microscopic variations in the crystal appear, see Fig. 1 (left and middle). These so-called *striations* can be measured even in the cooled-down crystal.

These striations can be measured via the *lateral photovoltage scanning* method (LPS) Lüdge and Riemann (1997). LPS excites the semiconductor crystal with a laser, creating a voltage difference at the sample edges which is proportional to the local doping variation. This opto-electrical measurement procedure detects doping inhomogeneities at wafer-scale and room temperature in a non-destructive fashion, see Fig. 1 (right). Interestingly, besides being very cost-effective and fast, this tabletop setup is—unlike other methods—especially suitable for low doping concentrations (10^{12} cm^{-3} to 10^{16} cm^{-3}) and thus applies to a large range of doping concentrations.

Even though we focus in this paper on measuring striations via the LPS method, the method itself may be applied in a considerably broader context. Any quantity that has an influence on the band edge energies may be visualized such as, for example, mechanical strain. Tauc predicted already in the 1950ies that the bulk photovoltaic effect, on which LPS relies, could be used to measure any physical quantity which affects the band structure of the material. This shows the potential of the LPS method. Unfortunately Tauc' assumptions (he considers for example a 1D sample) are not adequate for real measurements standards. To overcome these limitations Kayser et al. Kayser et al. (2018) simulate the LPS method for a given doping profile via a finite volume discretization of the van Roosbroeck system based on the commercial COMSOL Multiphysics toolbox. Eventually, one needs reconstruct the doping from the LPS measurements. However, for now we focus on computing the LPS voltage for a given doping. This step needs to be understood well before tackling the more complicated inverse problem. Unfortunately, the forward COMSOL simulation already requires long computation times to solve for the electron and hole densities, n, p, as well as the electric potential ψ. Additionally, it was not possible to simulate low doping concentrations.

To overcome these obstacles, we will rewrite the LPS model in terms of quasi Fermi potentials φ_n, φ_p and the electric potential ψ. We then proceed to introduce the laser profile, the sample inherent parameters of the recombination mechanisms and the charge carrier mobility model by Arora. We will also explicitly describe how we implement the nonlinear boundary conditions which models the circuit. We will discretize the nonlinear
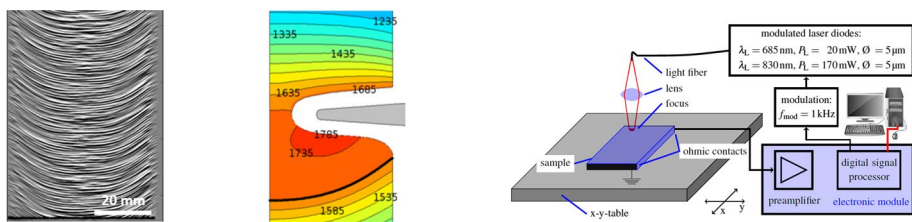

Fig. 1 Striations from LPS measurement (left); temperature field simulation created by a coil (the black line represents the solid-liquid interface at 1687K) (middle); LPS measurement setup (right). Temperature field simulation courtesy of Robert Menzel (Leibniz-Institut für Kristallzüchtung)

PDE system using a Voronoi finite volume method which we then implement via the open-source software tool `ddfermi` Doan et al. (2018). Our discretization approach is explained in greater detail in Farrell et al. (2020).

The aim of this paper is to study the underlying assumption of the LPS method that the LPS voltage is proportional to the doping variation. In particular, it is known that only for low injection conditions this proportionality can be mathematically justified. Here, we investigate for which laser powers this relationship is no longer true Farrell et al. (2020). In practice, understanding the limits of the LPS method is important because the method is known to produce unphysical output near the boundaries of the sample. In theory, this problem could be solved by choosing very large samples. However, to speed up the measurement process, one needs to choose the sample as small as possible. Hence, it is important make sure that boundary effects do not pollute the measurements for such small samples. Typically, there are two unphysical boundary effects: First, if both sample edges where the contacts are placed have different sizes, one needs to correct the signal accordingly. Second, the signal is distorted if too many charge carriers reach the contacts via diffusion. We focus on the second effect here which can also be simulated by increasing the laser power for a sample of fixed size. Finally, we provide an argument that lower local resolution for higher laser powers is caused by the screening effect of the generated charge carriers.

The rest of this paper is organized as follows: In Sect. 2 we introduce the model and in Sect. 3 its discretization. Finally, we present our results in Sect. 4 before we conclude in Sect. 5.

2 The van Roosbroeck model

In this section, we describe first the charge transport model. We model the silicon crystal as a bounded domain $\Omega \subset \mathbb{R}^2$. Its doping profile is given by the difference of donor and acceptor concentrations, $N_D(\mathbf{x}) - N_A(\mathbf{x})$, where $\mathbf{x} = (x, z)^T \in \Omega$.

The current densities for electrons and holes are given by $\boldsymbol{J}_n(\mathbf{x})$, $\boldsymbol{J}_p(\mathbf{x})$. These variables satisfy the following steady-state system, the so-called van Roosbroeck model,

$$-\nabla \cdot (\varepsilon \nabla \psi) = q(p(\psi, \varphi_p) - n(\psi, \varphi_n) + N_D(\mathbf{x}) - N_A(\mathbf{x}))$$

$$-\frac{1}{q} \nabla \cdot \boldsymbol{J}_n = G(\mathbf{x}) - R(\psi, \varphi_n, \varphi_p), \qquad \boldsymbol{J}_n = -q\mu_n n(\psi, \varphi_n) \nabla \varphi_n,$$

$$\frac{1}{q} \nabla \cdot \boldsymbol{J}_p = G(\mathbf{x}) - R(\psi, \varphi_n, \varphi_p), \qquad \boldsymbol{J}_p = -q\mu_p p(\psi, \varphi_p) \nabla \varphi_p. \tag{1}$$

The first equation is a nonlinear Poisson equation. The following two continuity equations describe the charge transport in a semiconductor crystal. Assuming Boltzmann statistics, the relations between the quasi-Fermi potentials and the densities of electrons and holes are given by

$$n(\psi, \varphi_n) = N_c \exp\left(\frac{q(\psi - \varphi_n) - E_c}{k_B T}\right), \quad p(\psi, \varphi_p) = N_v \exp\left(\frac{q(\varphi_p - \psi) + E_v}{k_B T}\right). \tag{2}$$

Here, we have denoted the conduction and valence band densities of states with N_c and N_v, the Boltzmann constant with k_B and the temperature with T. Furthermore, E_c and E_v refer to

the constant conduction and valence band-edge energies, respectively. Using relations (2) the current densities can be written in the following drift-diffusion form

$$J_n = -q\mu_n(n\nabla\psi - U_T\nabla n), \qquad J_p = -q\mu_p(p\nabla\psi + U_T\nabla p),$$

where $U_T = k_B T/q$ is the thermal voltage. The intrinsic carrier density n_i is defined via

$$n_i^2 = N_c N_v \exp\left(-\frac{E_c - E_v}{k_B T}\right). \tag{3}$$

If we neglect both transport equations, and only solve the nonlinear Poisson equation in (1) when no bias is supplied for the built-in potential ψ_{eq} and fixed quasi Fermi potentials $\varphi_n = \varphi_p = 0$, we say that the semiconductor is in *equilibrium*. The corresponding equilibrium charge densities n_{eq} and p_{eq} satisfy $n_{eq}p_{eq} = n_i^2$. Thus the doping concentrations enter the built-in potential ψ_{eq}. More informations regarding computational aspects of this approach can be found in Farrell et al. (2017). The stationary van Roosbroeck system is usually supplied with Dirichlet-Neumann type of boundary conditions.

2.1 Geometries

We will consider a 2D domain of silicon crystal. The sample has to be sufficiently longer than the mean free path of the electrons. Its necessary length depends on the assumed charge carrier life times but it can reach millimeter scale. The active region is highly centralized. For large charge carrier life times (millisecond range) it might be necessary to increase the sample length. The height of the sample is directly related to the penetration depth of the laser. For a laser with wave length $\lambda = 685$nm, the penetration depth is approximately 15nm. Thus our domain is given by

$$\Omega = \{(x, z) \in \mathbb{R}^2 \mid x \in [-\ell/2, \ell/2], z \in [-h, 0]\}$$

with $\ell = 3$mm and height $h = 5 \times 10^{-5}$mm. It is visualized in Fig. 2.

2.2 Generation rate

When a laser hits the crystal, some photons are reflected with constant reflectivity $\mathcal{R}$. The other *impinged* photons create electron and hole, resulting in a generation rate defined as follows

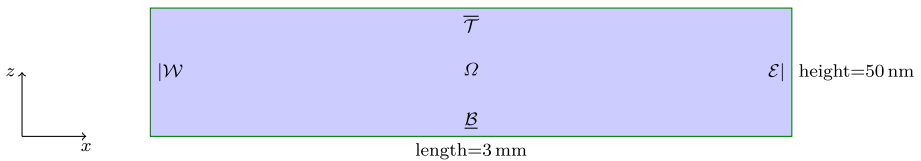$$G(\mathbf{x}) = N_{ph}(1 - \mathcal{R})S(\mathbf{x}), \tag{4}$$

Fig. 2 2D geometry of the simulated sample. The laser penetrates via $\overline{\mathcal{T}}$. In z-direction the laser power decreases with exponentially, see Eq. 5. In x-direction a Gaussian laser profile is assumed, see Eq. 6

where $S(\mathbf{x})$ is the shape function of the laser (normalized by $\int_\Omega S(\mathbf{x})d\mathbf{x} = 1$) and N_{ph} the impinging photon rate on the whole surface of the sample given by $N_{ph} = \frac{P_L \lambda_L}{hc}$. Here, P_L denotes the laser power, λ_L the wave length of the laser, $c = 3 \times 10^8$ m/s the speed of light in vacuum and $h = 6.6 \times 10^{-34}$ m^{2}kg/s $= 6.6 \times 10^{-34}$Js the Planck constant.

The shape function in 2D is given by $S(x, z) = S_x(x) \cdot S_z(z)$ where in z direction the absorption of the laser is assumed to decay exponentially

$$S_z(z) = \frac{1}{d_A} \exp\left[-\frac{|z|}{d_A}\right]. \tag{5}$$

Here d_A is the penetration depth, or in other words $1/d_A$ is the absorption coefficient, which heavily depends on the laser wave length. The shape function in x-direction is given by

$$S_x(x) = \frac{1}{\sqrt{2\pi}\sigma_L} \exp\left[-\frac{1}{2}\left(\frac{x - x_0}{\sigma_L}\right)^2\right], \tag{6}$$

where x_0 denotes the position of the laser along the x axis and σ_L the laser spot radius.

2.3 Recombination rates

The total recombination rate is given by the sum of the following three recombination rates,

$$R = R_{\text{dir}} + R_{\text{Aug}} + R_{\text{SRH}}$$
$$= C_d(np - n_i^2) + C_n n(np - n_i^2) + C_p p(np - n_i^2) + \frac{np - n_i^2}{\tau_p(n + n_T) + \tau_n(p + p_T)}, \tag{7}$$

i.e. the direct R_{dir}, Auger R_{Aug} and Shockley-Read-Hall R_{SRH} recombination rates.

2.4 Arora mobility model

The Arora mobility model takes into account the scattering of charge carriers with ionized impurities, most likely by doping. The electron and hole mobilities are given by

$$\mu_n = 89cm^2/Vs + \frac{1323 \text{ cm}^2/Vs}{1 + \left(\frac{N_D + N_A}{1 \times 10^{17} \text{ cm}^{-3}}\right)^{0.88}} \quad \text{and} \quad \mu_p = 55 \text{ cm}^2/Vs + \frac{429 \text{ cm}^2/Vs}{1 + \left(\frac{N_D + N_A}{1 \times 10^{17} \text{ cm}^{-3}}\right)^{0.88}}. \tag{8}$$

2.5 Coupling the device to an external circuit

So far we have modeled the silicon crystal but not the LPS setup itself. The electric current j_{D_i} flowing through the i-th ohmic contact Γ_{D_i} is defined by the surface integral

$$j_{D_i} = -\int_{\Gamma_{D_i}} \mathbf{v} \cdot (\mathbf{J}_n(\mathbf{x}) + \mathbf{J}_p(\mathbf{x}))d\sigma(\mathbf{x}), \qquad i = 1, 2. \tag{9}$$

According to the conservation of charge, the currents in (9) satisfy the relation $\sum_{i=1}^{2} j_{D_i} = 0$. For notational convenience we define

$$i_D := j_{D_1} = -j_{D_2}. \tag{10}$$

We model now the voltage meter as a simple circuit having a resistance R. The network has two nodes, in which the potentials are respectively u_{D_1} and u_{D_2}. Using the formalism of the Modified Nodal Analysis (MNA) we have that the difference between the electric potentials at the nodes is given by

$$u_{D_2} + \psi_0|_{\Gamma_{D_2}} - (u_{D_1} + \psi_0|_{\Gamma_{D_1}}) = \mathcal{R}\, i_D(u_{D_2}), \tag{11}$$

where i_D is defined in (10). Usually one of the nodes of an electric circuit is assumed to have an electric potential equal to the ground. This means in our case that we can arbitrarily set $u_{D_1} = u_{\mathrm{ref}} = 0$, and thus (11) reduces to

$$u_{D_2} + \Delta\psi_0 = \mathcal{R}\, i_D(u_{D_2}), \tag{12}$$

where $\Delta\psi_0 := \psi_0|_{\Gamma_{D_2}} - \psi_0|_{\Gamma_{D_1}}$.

Notice that (12) is an implicit equation for $u_{LPS} := u_{D_2}$ since i_D depends implicitly on u_{D_2}, via the van Roosbroeck system (1). Once we have found a solution $(\psi, \varphi_n, \varphi_p)$ to the van Roosbroeck system where u_{D_2} enters as a Dirichlet boundary condition, we compute the current i_D via (9). More details on this LPS model can be found in Farrell et al. (2020). More complicated models were analyzed analytically in Alì and Rotundo (2010).

3 Finite volume discretization

We partition our domain Ω into Voronoï cells ω_K such that $\Omega = \bigcup_{K=1}^{N} \omega_K$. Each control volume is associated with a node $\mathbf{x}_K \in \omega_K$. Via the divergence theorem we obtain after integration over each control volume a discrete version of the continuity equation in (1). Consistent with the continuous van Roosbroeck system, this *finite volume* discretization describes the change of the carrier density within a control volume. The corresponding numerical electron flux j_n describing the flow between neighboring control volumes can be expressed as a function, depending nonlinearly on the values $\psi_K, \psi_L, \eta_K, \eta_L$ such that

$$j_n(\psi_K, \psi_L, \eta_K, \eta_L) \approx \frac{1}{|\partial\omega_K \cap \partial\omega_L|} \int_{\partial\omega_K \cap \partial\omega_L} \boldsymbol{J}_n \cdot \boldsymbol{\nu}\, dS.$$

Here a function with subindex, e.g. K, denotes evaluation of the function at the node $\mathbf{x}_K$. More details can be found in Farrell et al. (2017),Farrell et al. (2017),Patriarca et al. (2018). We implement this discretization within the open-source software tool `ddfermiDoan` et al. (2018), which solves the nonlinear boundary condition (12) using a secant method Farrell et al. (2020).

4 Results

Tauc Tauc (1955) predicted, that the bulk photovoltaic effect, on which the LPS method relies, is proportional to small resistivity variations under low injection conditions. In particular, recently mathematical investigations Farrell et al. (2020) showed that

$$u_{LPS}(x_0) \propto -N_D'(x_0) \int_{x_0-\delta/2}^{x_0+\delta/2} \frac{1}{N_{D0}} \Delta\sigma(x-x_0)dx. \tag{13}$$

The authors concluded that if the integral in the above equation is approximately constant, then under certain assumptions specified in Farrell et al. (2020) the LPS voltage u_{LPS} is proportional to the doping gradient. Yet, especially close to the extrema of the doping gradient small discrepancies could be observed which the authors attributed to the approximations and assumptions used in deriving the approximate proportionality (13). In this paper, we are interested in how far the proportionality between LPS voltage and doping gradient is still satisfied even for extreme cases such as relatively high laser powers. Understanding this is also important for real LPS measurements as the signal will be polluted if too many charge carriers diffuse into the contacts. This may happen either if the sample is too small or the laser power too high. Figure 3 shows real LPS measurement data. Near the sample boundaries visual artifacts appear. The only reason that they are relatively modest in size is that the sample is relatively large. In practice, however, one would like to use relatively small samples to speed up the measurements. However, charge carrier diffusion imposes a natural limit on how small the samples may be chosen because if the charge carriers diffuse out of the sample one introduces an artificial dipole, resulting into these visual artifacts.

To understand the limits of (13), we investigate the effect of the laser power P on the LPS voltage u_{LPS}. Changing the laser power will change the conductivity variation $\Delta\sigma(x-x_0)$ for a constant average doping concentration N_{D0}. For sufficiently large laser powers, we will eventually violate the low injection conditions which was needed to prove (13). In Fig. 4a–d we show the behavior of simulated LPS scans with respect to the local doping gradient (right axis, red line) for various laser powers and the sinusoidal doping profile in (1) of the form

$$N_D(x) = N_{D0}\left(1 + A\sin\left(2\pi\frac{x}{L}\right)\right)$$

with an average doping value $N_{D0} = 1 \times 10^{16}$ cm^{-2}, an amplitude of $A = 0.2$ and a period of $L = 100\,\mu$m. As can be seen in Fig. 4 (a) the simulated LPS voltage perfectly matches the doping variation, which in turn is proportional to the resistivity variations Farrell et al. (2020). We present the LPS voltages without a non-physical offset, which as previously stated in Kayser et al. (2018) can be related to the sample geometry.

However, in Fig. 4b it can already be seen that the peak maxima and minima do not perfectly match the doping variation profile anymore. This effect even increases for higher laser powers, see Fig. 4c–d. The sinusoidal variation is superposed with an envelope function. This function might be explained by the larger diffusion of charge carriers, which are now able to reach the ohmic contacts. Therefore, the scan depends on the distance to the closest ohmic contact. Both contacts are placed at $x = \pm 1.5\,$mm.
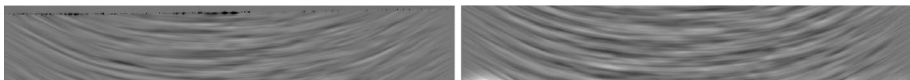

Fig. 3 Details from 2D LPS measurements for a 3D floating zone Silicon crystal performed at Leibniz-Institut für Kristallzüchtung (IKZ) with resistivity $\rho = 20\,\Omega$cm, average doping concentration of $N_{A0} = 6.51 \times 10^{14}$ cm^{-3} and a carrier life time of $\tau = 900\,\mu$s. The dimensions of the xy plane are $100\,$mm $\times 100\,$mm. At the top of the boundary sample (left figure), near the boundary, one can see visual artifacts in black. At the bottom of the boundary sample (right figure) one can see visual artifacts in white
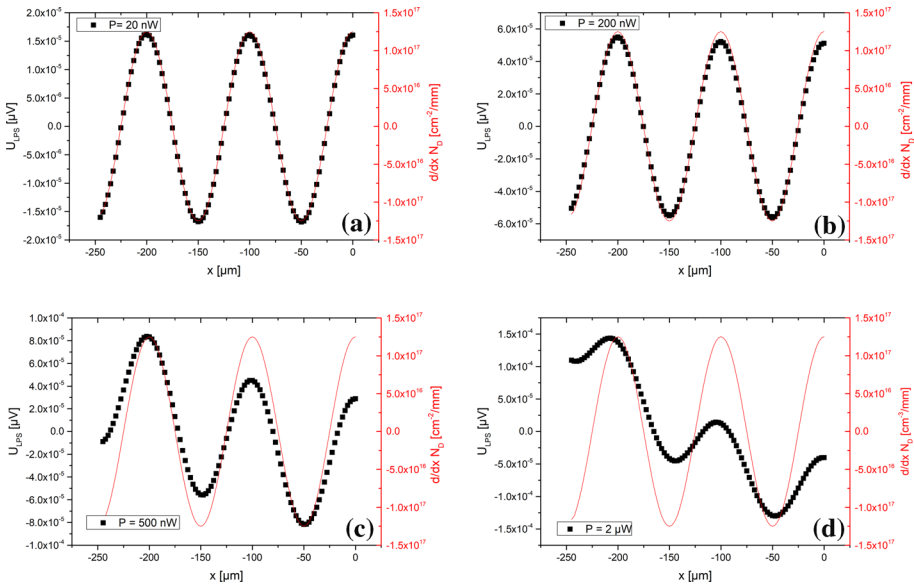
Fig. 4 Simulation of 1D LPS scans of a 2D silicon sample for different laser powers (**a–d**). The geometries and physical parameters are given in Sect. 2. In every plot, one finds the LPS signal in black (left x axis) and the spatially varying doping gradient in red (right x axis). For low laser powers around $P = 20$ nW the LPS voltage follows the doping gradient directly (a). In (b) for $P = 200$ nW small deviations can be observed. For high laser powers ($P = 500$ nW and $P = 2\,\mu$W) the screening effect will shield the LPS voltage resulting in a distorted signal(**c–d**)

Experimental results have shown that the local resolution of the LPS method is decreasing when increasing the laser power Lüdge and Riemann (1997). The behavior was attributed to an enlargement of the charge carrier cloud generated by a larger laser power. But as long as the mean free path for charge carriers remains constant, the convolving effect of this charge carrier cloud stays constant.

In Fig. 5, we show the ratio of LPS voltages and corresponding laser powers. For small laser powers (0.2 **nW** – 2 **nW**) the profiles are nearly overlapping, which indicates a linear dependency of the LPS voltage on the laser power in this regime. Only slightly reduced is the amplitude of the 20 **nW** profile (the same power used in Fig. 4b. For higher laser powers a large decrease in the amplitude can be observed, clearly showing that in this case the LPS voltage does not depend linearly on the laser power. It was shown analytically that this behavior is logarithmic and due to the screening effect of charge carriers Tauc (1955); Farrell et al. (2020).

Since in Fig. 4b the LPS profile begins to no longer match the doping variations and additionally in Fig. 5 the amplitude of the LPS voltage laser power ratio begins to decrease, these underlying physical effects might be connected. Therefore it is likely that the lower local resolution for higher laser powers is caused by the screening effect of the generated charge carriers. This also corroborates similar observations regarding the logarithmic relationship between LPS signal and laser power Tauc (1955),Farrell et al. (2020).

Fig. 5 LPS profiles normalized by the laser powers. For low laser powers the U_{LPS}/P_L ratio nearly overlapping (red and black curve). With increasing laser power the screening effect can be seen by a reduced u_{LPS}/P_L ratio
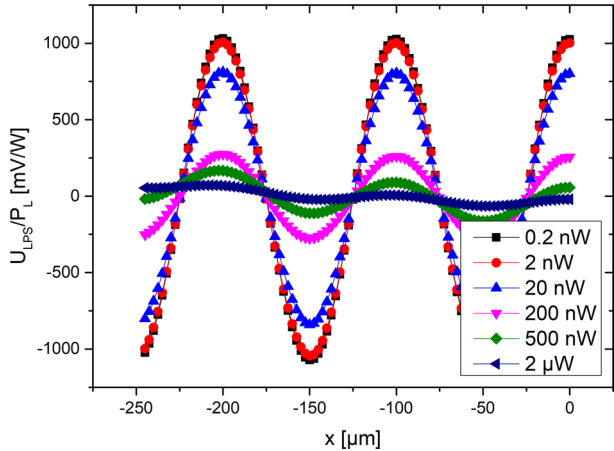
5 Conclusion

We presented simulations of the LPS measurement technique used to predict inhomogeneities in semiconductor crystals, using the open source software `ddfermi`. Due to flexibility of our approach, we were able to overcome efficiency and stability problems that a simulator based on commercial code has. By simulating several LPS profiles using low laser powers we could verify Tauc' assumptions that the bulk photovoltage is proportional to the doping gradient under certain conditions. Furthermore, we showed the limits of this proportionality with respect to higher laser powers. It appears that the loss in local resolution with increased laser power is connected to the screening effect of the generated charge carriers.

Authors' contribution All authors contributed to the study conception and design. Material preparation, data collection and analysis were performed by SK, NR and PF. The first draft of the manuscript was written by SK and all authors commented on previous versions of the manuscript. All authors read and approved the final manuscript.

Data availability and material The data can be obtained on demand.

Declarations

Conflict of interest Not applicable.

Code availability `ddfermi` is an open-source software prototype which simulates drift diffusion processes in classical and organic semiconductors Doan et al. (2018). Our code is available on demand.

References

Alì, G., Rotundo, N.: An existence result for elliptic partial differential-algebraic equations arising in semiconductor modeling. Nonlinear Anal.: Theory, Methods Appl. **72**(12), 4666–4681 (2010)

Becker, P., Pohl, H.J., Riemann, H., Abrosimov, N.: Enrichment of silicon for a better kilogram. Physica Status Solidi (a) **207**(1), 49–66 (2010)

Doan, D. H., Farrell, P., Fuhrmann, J., Kantner, M., Koprucki, T., Rotundo, N.: ddfermi—a drift-diffusion simulation tool. Version: 0.1.0, Weierstrass Institute (WIAS). (2018). http://doi.org/10.20347/WIAS.SOFTWARE.14

Farrell, P., Rotundo, N., Doan, D., Kantner, M., Fuhrmann, J., Koprucki, T.: Mathematical methods: drift-diffusion models. In: Piprek, J. (ed.) Handbook of Optoelectronic Device Modeling and Simulation, pp. 733–771. CRC Press, London (2017)

Farrell, P., Koprucki, T., Fuhrmann, J.: Computational and analytical comparison of flux discretizations for the semiconductor device equations beyond boltzmann statistics. J. Comput. Phys. **346**, 497–513 (2017)

Farrell, P., Kayser, S., Rotundo, N.: Modeling and simulation of the lateral photovoltage scanning method. WIAS Preprint **2784**, 1-24 (2020)

Kayser, S., Lüdge, A., Böttcher, K.: Computational simulation of the lateral photovoltage scanning method. *In: Proceedings of the 8th International Scientific Colloquium*, pp. 149–154, (2018)

Lüdge, A., Riemann, H.: Doping in homogeneities in silicon crystals detected by the lateral photovoltage scanning (LPS) Method. Inst. Phys. Conf. Ser. **160**, 145–148 (1997)

Patriarca, M., Farrell, P., Fuhrmann, J., Koprucki, T.: Highly accurate quadrature-based Scharfetter–Gummel schemes for charge transport in degenerate semiconductors. Comput. Phys. Commun. **235**, 40–49 (2018)

Tauc, J.: The theory of a bulk photo-voltaic phenomenon in semi-conductors. Czechosl. Fiziceskij Zurnal **5**, 178–191 (1955)

Zulehner, W.: The growth of highly pure silicon crystals. Metrologia **31**(3), 255–261 (1994)